Robust One-pot Synthesis of Citrate-Stabilized $Au@CeO_2$ Hybrid Nanocrystals with Different Thickness and Dimensionality.

Neus G. Bastús*[, 1], Jordi Piella[1], Sara Perez[1], Javier Patarroyo[1], Aziz Genç[1], Jordi Arbiol[1, 2] and Victor Puntes*[, 1, 2,3]

[1] Institut Català de Nanociència i Nanotecnologia (ICN2), CSIC, The Barcelona Institute of Science and Technology (BIST), Campus UAB, Bellaterra, Barcelona, Spain.

[2] Institució Catalana de Recerca i Estudis Avançats (ICREA), 08010 Barcelona, Spain.

[3] Vall d'Hebron Institut de Recerca (VHIR), 08035, Barcelona, Spain.

* To whom correspondence should be addressed: E-mail: neus.bastus@icn2.cat, victor.puntes@icn2.cat

ABSTRACT

Well-defined colloidal $Au@CeO_2$ hybrid nanocrystals (NCs) comprising different core/shell morphologies have been synthesized via a novel and simple one-pot aqueous approach. The method allows producing hybrid morphologies composed by an active and accessible Au core coated by a porous CeO_2 shell with varying shell thickness and dimensionality by simply adjusting the Au^{3+}/Ce^{3+} precursor ratio. These hybrid NCs are highly monodisperse and well-dispersed in water, showing intense surface plasmon resonance bands that offer unique opportunities for advanced material applications, such as plasmonics and catalysis.

INTRODUCTION

Controllable integration of noble metals and metal oxides into single nanostructures has recently become one of the hottest research topics due to the unique structural features and synergetic optical and catalytic properties that these complex NCs possesses [1-4]. In quest of developing advanced functional NCs, the design of metal-oxide nanostructures has become quite sophisticated through controlling the size, shape and crystal structure of the constituent domains. Still, a long-standing barrier has been the development of simple and cost-effective synthetic processes allowing a fine adjustment of the structure and interface of these systems [5]. Until now, a great deal of work has been performed to design and produce different nanostructures containing noble metal (Pt, Pd, Au, Ag) cores and CeO_2 shells with outstanding optical and catalytic properties [6-10]. However, the synthetic protocols for the production of these NCs have become considerably more and more complicated as the control of NC's morphology and architecture becomes more precise, often requiring multiple steps and exotic techniques [7, 11]. This achievement is particularly challenging in the case of $Au@CeO_2$ NCs systems due to the difficulties in balancing effectively the heterogeneous nucleation and growth of CeO_2 onto Au cores due to its low affinity and strong immiscibility [12-16].

Among wet-chemistry strategies, the preparation of $Au@CeO_2$ NCs by one-pot methods are especially interesting since they permit simplification of the overall synthetic procedure, allow a better reproducibility and avoid time-consuming processes, which is of special interest when industrial purposes are concerned. However, despite their interest, there are very limited reports on the formation of $Au@CeO_2$ NCs by one-pot techniques due to the difficulties in controlling the homogeneous nucleation and growth processes of the different materials by simply adjusting reaction parameters. A remarkable example was reported by Kaneda and co-workers, who described the controlled production of small $Au@CeO_2$ core-shell NCs (< 20 nm) in a single step by a redox co-precipitation method [17]. Advantageously, this route allows producing well-defined structures with remarkable optical and catalytic properties by the direct mutual oxidation (Ce^{3+} to Ce^{4+}) and reduction (Au^{3+} to Au^0) of the precursors involved in the reaction [7, 17]. Despite the appeal of such an approach, the final morphology and composition of the NCs are determined by the electronic stoichiometry of the reaction and precursor reduction potential, hindering any control over the NC's morphology. Alternatively, Tang et al. [18] proposed a one-pot hard-templating method for the production of sub-micrometric hybrid NCs. In this case, the use of additional reducing agents allowed for a better control of the morphology of the system but a calcination step is required to obtain the hybrid nanostructure. Remarkably, in both cases, the reaction resulted in a black-brown suspension, indicating the poor stability and significant polydispersity of the resultant NCs, not suitable for optical applications.

In this context, there is a current need to develop synthetic methods for the production of stable colloidal solutions of Au@CeO_2 hybrid NCs allowing adjusting the morphological characteristics of the structure, especially shell thickness and dimensionality, whose control remains still a challenge. Dimensionality is important because uncompleted shells (clover-like) will maximize Au-CeO_2 interfaces generating anisotropic distributions of the electric field suitable for plasmonics and catalysis [15, 19]. Herein, we address this problem presenting a general, straightforward and simple one-pot aqueous approach for the preparation of nearly monodisperse Au@CeO_2 NCs. The method allows producing hybrid morphologies composed by an active and accessible Au core coated by a porous CeO_2 shell with varying shell thickness and dimensionality by simply adjusting the Au^{3+}/Ce^{3+} precursor ratio. This synthetic strategy, based on the identification of the experimental conditions under which both components are grown *in situ* and self-regulate into a single nanostructure, allows a high quality, reproducibility and avoids time-consuming processes. Remarkably, the absence of any calcination step in our method facilitates the control of the overall NC morphology while circumventing aggregation and sintering problems occurring during post-synthesis thermal treatments. As a result, NCs remain well-defined and dispersed in solution which is highly beneficial for the control of their properties and plasmonic functionality.

RESULTS and DISCUSSION

Synthesis of Au@CeO_2 Hybrid Nanocrystals

Colloidal solutions of highly monodisperse Au@CeO_2 NCs were obtained by the reaction between $HAuCl_4$ (1 mL, 25 mM) and $Ce(NO_3)_3$ (5 mL, 25 mM) in a refluxing aqueous solution of sodium citrate (SC) (100 mL, 10 mM) during four hours of reaction. All the reagents required to form the NCs were present in the solution from the beginning and the reaction was driven by a kinetically-controlled nucleation and growth process under the appropriate conditions (temperature, pH and precursor/surfactant ratios) [20, 21].

Representative images of transmission electron microscopy (TEM) and high-angle annular dark field scanning TEM (HAADF-STEM) of as-obtained colloidal solutions are shown in **Figure 1A-C.** Obtained results show the systematic formation of Au@CeO2 NCs consisting of an Au core (~5 nm) surrounded by a relatively uniform CeO_2 shell. Notice that the Au core presents a brightest contrast in the HAADF-STEM images due to the Z-contrast. Unlike other common shell components with a continuous phases [22] -such as SiO_2,TiO_2, Cu_2O and ZnO- the CeO_2 layer is not compact nor continuous, indicating that the growth of CeO_2 follows Volmer–Weber growth modes, as expected from the large mismatch of lattice parameters between CeO_2 (0.5412 nm) and Au (0.4065 nm). Remarkably, we did not observe the formation of any isolated CeO_2 or Au NCs

in the product, which is a further indication of the self-controlled Au@CeO_2 NC's formation process.

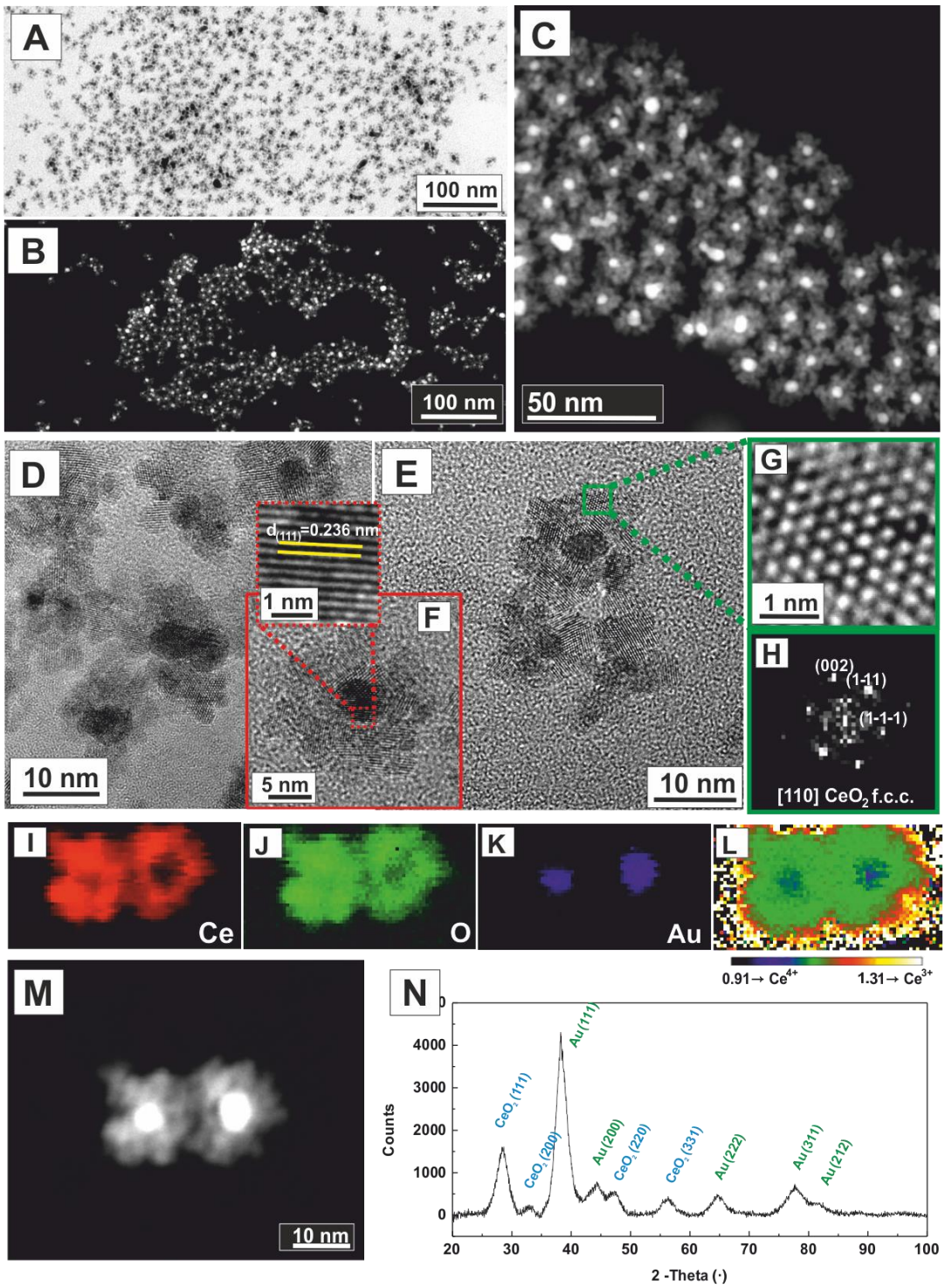

Figure 1. Synthesis of Au@CeO_2 Hybrid Nanocrystals. Representative Transmission Electron Microscopy (TEM) images (**A**) and high-angle annular dark field scanning TEM (HAADF-STEM) images (**B-C**) of as-obtained colloidal Au@CeO2 hybrid NCs, revealing the formation of a core of Au (~5 nm) surrounded by a relatively uniform CeO_2 shell. High-resolution TEM (HRTEM) images (**D-F**) revealing the details of the CeO_2 shell, which is composed of small NCs with sizes around 2-3 nm closely bound to the Au core. Inset in **(F)** reveals the (111) planes of face-centered cubic Au phase. Detail of the green squared CeO_2 region **(G)** and its corresponding

power spectrum **(H)**, showing the f.c.c crystalline structure of the CeO_2 NCs. Electron energy-loss spectroscopy (EELS) elemental maps (**I-L**) obtained from the hybrid NCs shown in the HAADF-STEM image (**M**). Map of L3/L2 EELS edges intensity ratio (**L**) reveals the oxidation states of Ce. X-ray diffraction (XRD) patterns of hybrid Au@CeO_2 NCs (**N**).

According to HRTEM images (**Figure 1D-F**), the shell is composed of tiny CeO_2 NCs with sizes between 2-3 nm, closely bound to the Au core. This suggests a strong interfacial interaction between the CeO_2 and Au cores that often results in favor of their optical and catalytic properties [7, 17]. Details of the squared region (**Fig. 1G**) and its corresponding power spectrum (**Fig. 1H**) reveals that the CeO_2 NCs are crystalline. The elemental chemical composition maps obtained by electron energy-loss spectroscopy (EELS) (**Figure 1 I-M**) corroborate the encapsulation of the metal core by CeO_2. The map of the intensity ratio of L_3 edge peak over L_2 edge peak from **Figure 1L** reveals that the CeO_2 shell is composed by a mixture of Ce^{4+} and Ce^{3+}, with its inner part rich in Ce^{4+} and its outer part composed by Ce^{3+} [23, 24]. Once discarding beam effects, this is attributed to the presence of the Au core acceptor.

The crystal structure of the Au@CeO_2 NCs was further investigated by X-ray diffraction (XRD) (**Figure 1N).** Two series of sets of diffraction peaks are present, which are assigned to the fluorite (cubic) CeO_2 phase (JCPDS No 34-0394) and to the cubic Au phase (JCPDS No 04-0784). The diffraction peaks of the Au core are sharp and intense, while those of CeO_2 are broad and weak, accordingly with the small crystalline size of the CeO_2 NCs composing the shell. The crystalline sizes of CeO_2 (3.4 nm) and Au (4 nm) calculated from the XRD data are consistent with those obtained by TEM analysis.

In our approach, simple adjustments of the Au^{3+} to Ce^{3+} precursor ratio allowed controlling the final morphology of the hybrid structure. Thus, by increasing the amount of Ce^{3+} injected from ratio 1:1 to 1:6 while keeping constant the other reaction parameters, the CeO_2 shell thickness was precisely adjusted from ~ 2.2 nm to ~ 12 nm while the size of the Au core remained constant at ~5.5 nm (**Fig. 2A-E, Fig. S1**). Interestingly NCs with thinnest CeO_2 layers -corresponding to 1:0.5 and 1:1 ratio- are clover-like structures presenting a lower dimensionality than those produced at higher ratios, which ultimately maximizes the Au-CeO_2 interface. In all cases, samples present a great stability in water, showing vivid colors from red to purple depending on the CeO_2 thickness.[17] (**Fig. 2F**). The impact of the CeO_2 coating in the localized surface plasmon resonance (LSPR) of Au cores was studied by UV-Vis spectroscopy (**Fig. 2G, Fig. S2)**. Citrate-stabilized Au NCs of a similar core were also prepared for comparison [25]. Interestingly, three distinct features in the spectra upon the CeO_2 coating can be clearly seen: i) the increase of the well-defined absorption of CeO_2 in the near ultraviolet region -interband transitions-, ii) the systematic red-shift from 514.5 nm to 555 nm of the LSPR Au peak position as the overall CeO_2 thickness increases and iii) the progressive broadening of the plasmon band (**Table 1**). These

results can be explained by the increased refractive index (n≈ 2.2) of the dielectric environment surrounding the Au cores upon CeO_2 coating that results in a red-shift whose extension depends on the thickness and degree of coating of the Au cores. Thus, non-uniform clover-like Au@CeO_2 NCs, where parts of the Au surface are exposed to water, experience smaller red-shifts than NCs with a uniform and thick CeO_2 coating around the Au cores [26]. Remarkably, for the thicker shells measured, the SPR shift reaches a maximum value where it saturates. This phenomenon, widely reported for the other similar systems, relates to the maximum distance to which the local field extends from NP's surface [27, 28]. Similarly, the broadening of the plasmon band as the CeO_2 shell thickness increases can be associated with the non-compact nature of the CeO_2 shell coating. Thus, as the shell increases in thickness its "density and compactness" decreases which correlates with the observed band broadening.

With the aim of gaining further insight into the impact of the CeO_2 coating on the optical properties of Au NCs, extinction efficiencies of an Au sphere of 5 nm of varying CeO_2 coatings have been calculated following the standard Mie [29] **(Fig. S3)**. Despite the good correlation between experimental results and Mie calculations, the calculated SPR red-shits are systematically larger than those experimentally obtained. These differences are mainly attributed to the "compactness" of the CeO_2 shell. Thus, we certainly assume that Au NCs are surrounded by a dense CeO_2 coating layer while experimental results suggest that the CeO_2 shell is rather porous and low dense. This assumption determines the effective dielectric constant of the system, which ultimately affects the extent on the SPR red-shifts.

Table 1: NC sizes and SPR peaks depending on the precursors Au^{3+}/Ce^{3+} molar ratio

Ratio Au^{3+}:Ce^{3+}	**Au Core size (nm)**	**Overall size (nm)**	**CeO_2 Shell Thickness**	**SPR (nm)**
Au cores[25]	5.7 ± 1.3	-----		514.5
1:0.5	5.2 ± 1.3	7.8 ± 2.3	2.6 ± 3.6	520.5
1:1	5.3 ± 1.4	9.6 ± 1.6	4.3 ± 3.0	532.5
1:2	5.6 ± 1.4	11.5 ± 1.9	5.9 ± 3.3	542.5
1:4	5.4 ± 1.0	12.9 ± 2.7	7.5 ± 4.7	551.5
1:6	5.2 ± 1.3	16.5 ± 3.1	11.3 ± 4.4	555.0

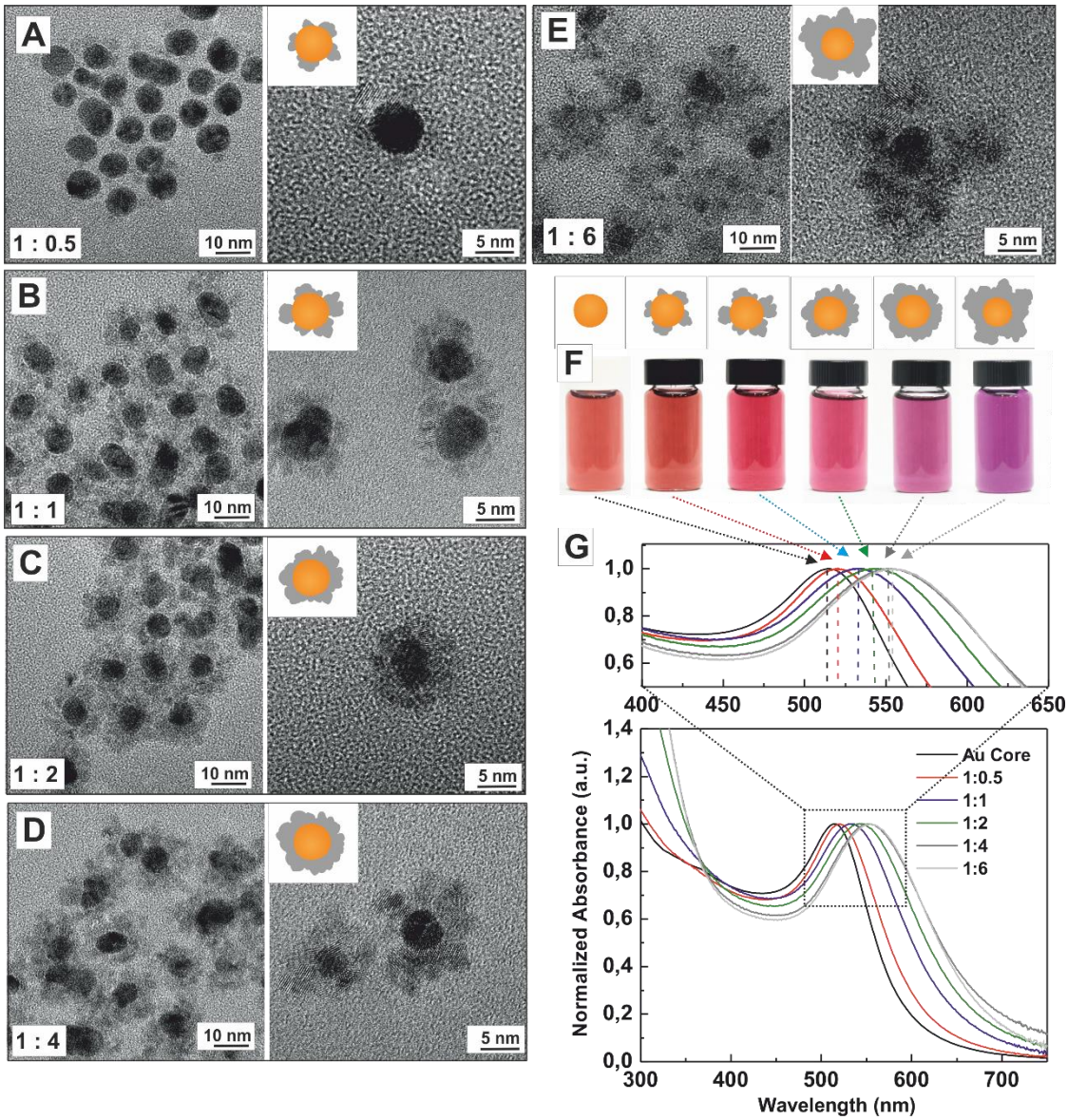

Figure 2. Control of the CeO_2 shell thickness in Au@CeO_2 Hybrid NCs. Representative TEM images of well-defined Au@CeO_2 hybrid NCs with increasing shell thicknesses achieved by adjusting the Au^{3+}/Ce^{3+} molar ratio from 1:0.5 (**A**) to 1:1 (**B**), 1:2 (**C**), 1:4 (**D**) and 1:6 (**E**). Images of colloidal solutions of Au and Au@CeO_2 hybrid NCs with increasing shell thicknesses (**F**). Variations of the thickness of the CeO_2 shell from ~ 2.2 nm to ~ 12.1 nm are translated into a red-shift of the SPR position from 514.5 nm (Au NCs) to 520.5 nm (ratio 1:0.5), 532.5 nm (ratio 1:1), 542.5 nm (ratio 1:2), 551.5 nm (ratio 1:4), and 555 nm (ratio 1:6) (**G**).

The possibility to precisely adjust the thickness of the CeO_2 shell is of crucial importance for tailoring the final functionality of these systems [30]. On the one side, the use of core/shell plasmonic structures in fluorescence enhancement and surface-enhanced Raman scattering (SERS) requires the study of the optimum shell thickness for obtaining the maximum near-field enhancement at the core-shell and shell–medium interfaces [28]. Moreover, the plasmonic enhancement is particularly interesting for the study of plasmon resonances at their fundaments,

including nonlinear optical processes such as second harmonic generation [31]. In this regard, one of the main advantages of CeO_2 as a shell material compared to other oxides, e.g. SiO_2, is its higher refractive index. Thus, when the Au cores are coated with a CeO_2 dielectric shell of a certain thickness, the SPR position shifts to longer wavelengths than that corresponding to identical SiO_2-coated Au cores (**Fig. S3**) [27]. On the other side, the precise adjustment of shell thickness allows for the proper balance of the stability of the NCs and the accessibility of the inner metal core. Thus, while a thick CeO_2 shell may difficult the access of some type of substrate molecules to reach the surface of the noble metal core, a too thin CeO_2 shell may compromise the sintering of the noble metal core, especially for size below 6 nm. [18] Indeed, the accessibility of the inner metal core in the thicker Au@CeO_2 structures was proved by studying the catalytic degradation of 4-nitrophenol (4-NP) by borohydride ions (**Fig. S4**). [32] Although a decrease of the reduction rate of the dye is observed for Au@CeO_2 NCs in comparison to bare Au NCs of similar core sizes, the presence of the thick CeO_2 shell does not prevent the 4-NP from reaching the inner metal core.

Formation Mechanism

To determine the formation mechanism of the Au@CeO_2 hybrid NCs, we monitored the process by extracting aliquots at different reaction times after the initialization event, which is the addition of the Au^{3+} precursor to the aqueous Ce^{3+}/SC mixture. Evidence of hybrid NC formation can be seen by monitoring the temporal evolution of the UV-Vis spectra (**Fig. 3-A**). At short reaction times, the appearance of an intense absorption band peaking at ~515 nm indicates the primary formation of small (5-6 nm) Au NCs.[33] From that moment on, the characteristic absorption of CeO_2 in the near ultraviolet region gets defined and systematically increases in accordance with the formation of the CeO_2 NCs (**Fig. 3-B**). This process takes place slowly at the surface of Au NCs, as indicated by the red-shift of the SPR peak position (**Fig. 3-C**) [34]. Interestingly, the extent of the reaction was seen to depend largely on the Ce^{3+} concentration, suggesting that the CeO_2 coating thickness increases as much as there is Ce^{3+} precursor in solution. At longer reaction times (up to 5 hours) only slight changes were observed.

Morphological analysis of same aliquots by TEM provides additional information about the formation mechanism of the Au@CeO_2 heterostructured NCs (**Fig. 3-D**). At short reaction times, the sample is mainly composed by worm-like Au NCs, with no evidence of the CeO_2 coating. The presence of these anisotropic Au morphologies, widely reported in the literature as mixed intermediate Au(I) products in the citrate-mediated synthesis of Au NCs [35, 36], suggests the primary reduction of Au^{3+} by the SC [37, 38]. Then, the progressive nucleation of some small undefined CeO_2 NCs can be seen at the Au surface (60-120 minutes). After another 3 hours of

reaction, the shell grows large and becomes more continuous. Finally, at long reaction times (5 h), a complete shell is formed onto the surface of the Au core and only slight changes are observed.

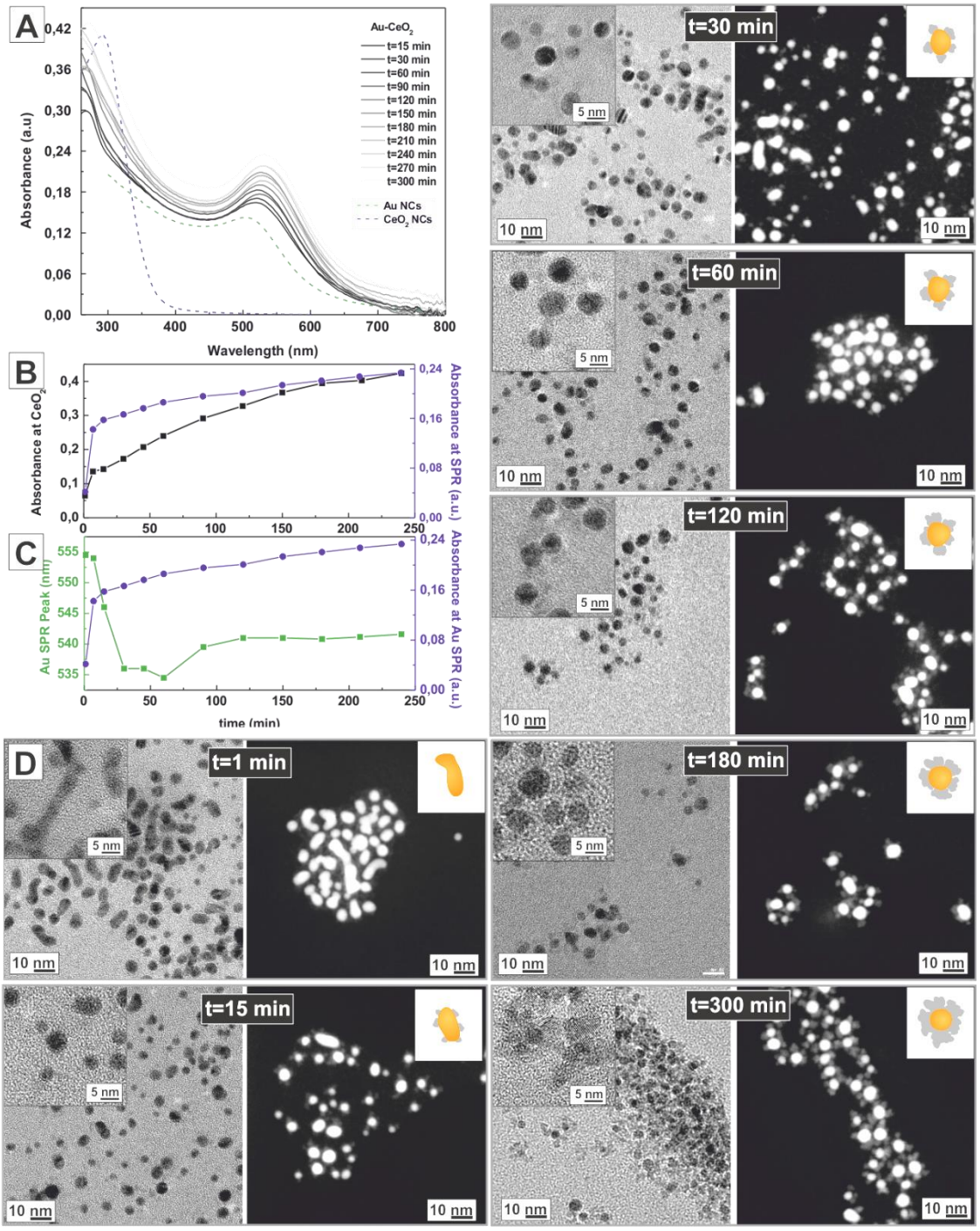

Figure 3. Representative TEM images and corresponding extinction spectra of Au@CeO_2 NCs obtained at different reaction times (A). At short reaction times, samples are mainly composed by anisotropic worm-like Au NCs, with no evidence of the CeO_2 coating. These intermediates species of the reaction subsequently evolve into well-defined quasi-spherical Au NCs encapsulated by a CeO_2. The CeO_2 thickness progressively increases as the reaction process leading to well-defined Au@CeO2 hybrid NCs. **Temporal evolution of Au@CeO_2 Hybrid NCs Formation**. UV–vis spectra of Au@CeO2 hybrid NC growth at different reaction times **(B)**. Time evolution of the intensity maximum of CeO_2 (290 nm) and Au (SPR band) as a function of time

(**C**). Time evolution of the SPR band position and the intensity maximum of Au as a function of time (**D**). The increase in absorption at CeO_2 peak position together with the red-shift of the SPR indicates the formation of a well-defined CeO_2 shell onto the Au NCs formed at the early stages of the reaction.

Despite the limitations of this ex situ approach, obtained results provide a valuable information to properly evaluate the formation mechanism of hybrid NCs [39]. Thus, the above analysis suggests that the formation of Au@CeO_2 NCs can be described in terms of the initial formation of Au cores and the subsequent slow oxidation and posterior hydrolysis of Ce^{3+} ions, catalyzed at the surface of the metal. In these processes, SC plays multiple roles, acting as a reducer and stabilizer in the formation of Au NCs and as a pH buffer (~6.5). In this regard, we found that keeping the pH of the solution at alkaline values is of crucial importance in the formation of the CeO_2 NCs. Thus, no shell was observed when performing the reaction at acidic pH (5.5), which was attributed to the low reactivity of Ce^{3+} in these conditions to be oxidized to Ce^{4+} and precipitate (**Fig. S5**).

Interestingly, the Au cores in the obtained hybrid structure (~5 nm) are much smaller than that expected by the direct citrate reduction of Au^{3+} (~10 nm). One may speculate that the early formed Au NCs became fast coated by the CeO_2 shell, restricting their further growth. However, as previously stated, the CeO_2 shell is porous, offering pathways to access the Au core. Therefore, results suggest that Ce^{3+} ions act as a secondary reducer, promoting the faster nucleation of a larger number of smaller metal cores [25]. This point is supported by the fact that Au NC formation kinetics are faster in the Ce^{3+}-citrate mixture than in a pure citrate solution. Remarkably, under the experimental conditions studied, the size of the Au NCs is not determined by the concentration of the reducers but by their reducing strength. This is translated into the fact that Au core diameter does not decrease as the cerium concentration is increased. Finally, we also evaluated the synthesis of Au@CeO_2 NCs in the absence of SC (**Fig. 4**). In these conditions, the color of the $Ce(NO_3)_3$/$HAuCl_4$ solution mixture remains transparent/light green even after 5 hours of reaction (**Fig 4A-B**) with a small precipitate at the bottom whose TEM analysis revealed the presence of a mixture of larger Au structures decorated with some small CeO_2 NCs. The subsequent addition of SC turns out into a sudden color change (from light green to purple) which is ascribed to the reduction of Au^{3+} ions not previously reduced by Ce^{3+} (**Fig. 4C**). These results suggest that although the oxidation (Ce^{3+}/Ce^{4+}) – reduction (Au^{3+}/Au^0) precursors are partially driven by a redox process, the presence of SC is needed to convert all Au^{3+} precursor and form homogeneous and colloidal-stable Au@CeO_2 NCs. Additionally, by decoupling the reduction of Au from the oxidation of Ce, it is possible to get a deeper control of the system and adjust the thickness of the CeO_2 as previously detailed.

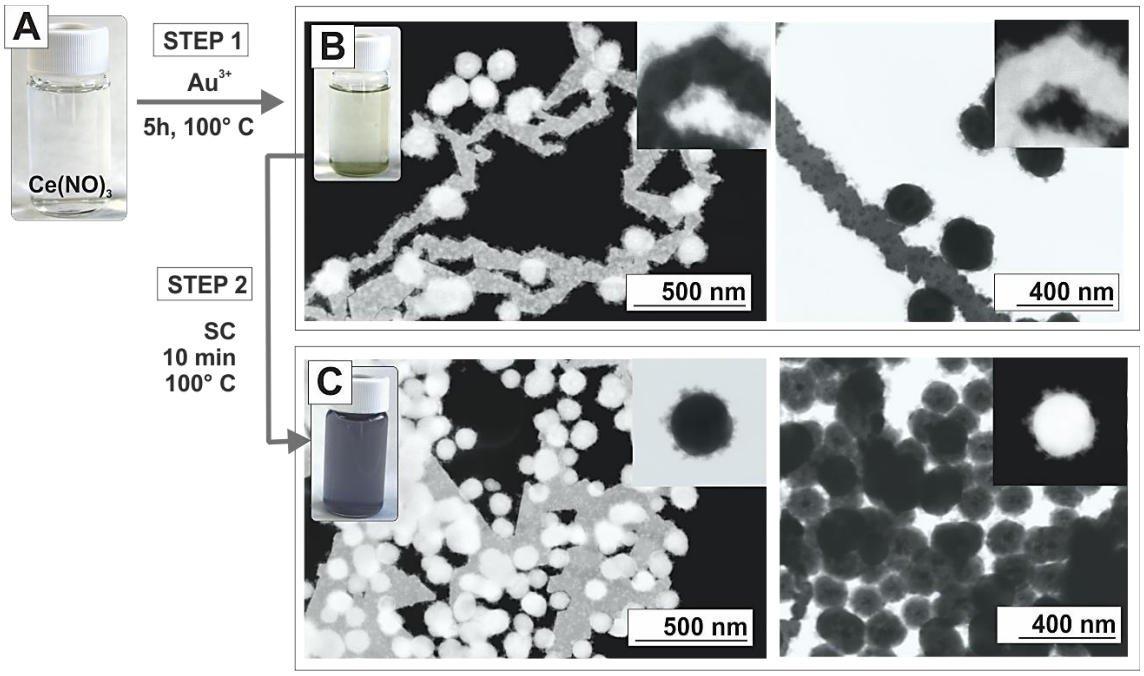

Figure 4. Formation Mechanism of Au@CeO2 Hybrid NCs in the Absence of Sodium Citrate. When Au^{3+} is used as direct oxidizer agent for the Ce^{3+} ions, the color of the $Ce(NO_3)_3/HAuCl_4$ solution mixture remains transparent/light green even after 5 hours of reaction (**A-B**). TEM analysis reveals the presence of a mixture of Au structures decorated with some CeO_2 small NCs. Subsequent addition of SC turns out into a sudden color change (from light green to purple) ascribed to the reduction of Au^{3+} ions not previously reacted (**C**).

Conclusions

To summarize, herein we reported a general, straightforward and robust simple one-pot aqueous approach for the preparation of stable colloidal solutions of $Au@CeO_2$ NCs that allows producing core/shell morphologies with varying shell thickness and dimensionality by simply adjusting the Au^{3+}/Ce^{3+} precursor ratio. This synthetic strategy relies on the use of sodium citrate as a reducer, pH buffer and stabilizing agent, and the identification of the experimental conditions under which both components are growth *in situ* and self-regulate into a single nanostructure. Besides, the resultant NCs are stable, well-dispersed in water and highly monodisperse which allows studying the impact of fine variations of the hybrid nanostructure on the underlying optical response. It is believed that such a stable hybrid NCs and the facile synthesis strategy using only biocompatible reagents have great potential for applications in the future.

Acknowledgments

We acknowledge financial support from the Spanish MINECO (MAT2015-70725-R, ENE2017-85087-C3) and from the Catalan Agència de Gestió d'Ajuts Universitaris i de Recerca (AGAUR) (2017-SGR-1431, 2017-SGR-327). Financial support from the HISENTS (685817) Project financed by the European Community under H20202 Capacities Programme is gratefully acknowledged. N.G.B. acknowledges financial support by MINECO through the Ramon y Cajal

program (RYC-2012- 10991). ICN2 is supported by the Severo Ochoa program from Spanish MINECO (Grant No. SEV-2017-0706) and is funded by the CERCA Programme / Generalitat de Catalunya. Part of the present work has been performed in the framework of the Universitat Autònoma de Barcelona Degree and Ph.D. program.

REFERENCES

[1] G. Li, Z. Tang, Noble metal nanoparticle@metal oxide core/yolk-shell nanostructures as catalysts: recent progress and perspective, Nanoscale, 6 (2014) 3995-4011.

[2] T. Mitsudome, K. Kaneda, Advanced Core–Shell Nanoparticle Catalysts for Efficient Organic Transformations, ChemCatChem, 5 (2013) 1681-1691.

[3] N.S. Sobal, M. Hilgendorff, H. Möhwald, M. Giersig, M. Spasova, T. Radetic, M. Farle, Synthesis and Structure of Colloidal Bimetallic Nanocrystals: The Non-Alloying System Ag/Co, Nano Lett., 2 (2002) 621-624.

[4] N. Pazos-Pérez, B. Rodríguez-González, M. Hilgendorff, M. Giersig, L.M. Liz-Marzán, Gold encapsulation of star-shaped FePt nanoparticles, J. Mater. Chem., 20 (2010) 61-64.

[5] S. Liu, S.-Q. Bai, Y. Zheng, K.W. Shah, M.-Y. Han, Composite Metal–Oxide Nanocatalysts, ChemCatChem, 4 (2012) 1462-1484.

[6] Q. Tan, C. Du, Y. Sun, G. Yin, Y. Gao, Pd-around-CeO2-x hybrid nanostructure catalyst: three-phase-transfer synthesis, electrocatalytic properties and dual promoting mechanism, J. Mater. Chem. A, 2 (2014) 1429-1435.

[7] B. Li, T. Gu, T. Ming, J. Wang, P. Wang, J. Wang, J.C. Yu, (Gold Core)@(Ceria Shell) Nanostructures for Plasmon-Enhanced Catalytic Reactions under Visible Light, ACS Nano, 8 (2014) 8152-8162.

[8] C. Zhang, S. Li, T. Wang, G. Wu, X. Ma, J. Gong, Pt-based core-shell nanocatalysts with enhanced activity and stability for CO oxidation, Chemical Communications, 49 (2013) 10647-10649.

[9] T. Mitsudome, Y. Mikami, M. Matoba, T. Mizugaki, K. Jitsukawa, K. Kaneda, Design of a Silver–Cerium Dioxide Core–Shell Nanocomposite Catalyst for Chemoselective Reduction Reactions, Angewandte Chemie International Edition, 51 (2012) 136-139.

[10] H.-P. Zhou, H.-S. Wu, J. Shen, A.-X. Yin, L.-D. Sun, C.-H. Yan, Thermally Stable Pt/CeO2 Hetero-Nanocomposites with High Catalytic Activity, J. Am. Chem. Soc., 132 (2010) 4998-4999.

[11] Y.H. Qu, F. Liu, Y. Wei, C.L. Gu, L.H. Zhang, Y. Liu, Forming ceria shell on Au-core by LSPR photothermal induced interface reaction, Appl. Surf. Sci., 343 (2015) 207-211.

[12] M.S. Chen, D.W. Goodman, The Structure of Catalytically Active Gold on Titania, Science, 306 (2004) 252-255.

[13] P.X. Huang, F. Wu, B.L. Zhu, X.P. Gao, H.Y. Zhu, T.Y. Yan, W.P. Huang, S.H. Wu, D.Y. Song, CeO2 Nanorods and Gold Nanocrystals Supported on CeO2 Nanorods as Catalyst, J. Phys. Chem. B, 109 (2005) 19169-19174.

[14] S. Carrettin, P. Concepcion, A. Corma, J.M.L. Nieto, V.F. Puntes, Nanocrystalline CeO2 increases the activity of an for CO oxidation by two orders of magnitude, Angewandte Chemie-International Edition, 43 (2004) 2538-2540.

[15] N.J. Divins, I. Angurell, C. Escudero, V. Pérez-Dieste, J. Llorca, Influence of the support on surface rearrangements of bimetallic nanoparticles in real catalysts, Science, 346 (2014) 620-623.

[16] A. Trovarelli, Catalytic properties of ceria and CeO2-containing materials, Catal Rev, 38 (1996) 439-520.

[17] T. Mitsudome, M. Yamamoto, Z. Maeno, T. Mizugaki, K. Jitsukawa, K. Kaneda, One-step Synthesis of Core-Gold/Shell-Ceria Nanomaterial and Its Catalysis for Highly Selective Semihydrogenation of Alkynes, J. Am. Chem. Soc., 137 (2015) 13452-13455.

[18] J. Qi, J. Chen, G. Li, S. Li, Y. Gao, Z. Tang, Facile synthesis of core-shell Au@CeO2 nanocomposites with remarkably enhanced catalytic activity for CO oxidation, Energy & Environmental Science, 5 (2012) 8937-8941.

[19] A. Yazdi, A. Abo Markeb, L. Garzón-Tovar, J. Patarroyo, J. Moral-Vico, A. Alonso, A. Sánchez, N. Bastus, I. Imaz, X. Font, V. Puntes, D. Maspoch, Core–shell Au/CeO2 nanoparticles supported in UiO-66 beads exhibiting full CO conversion at 100 °C, J. Mater. Chem. A, 5 (2017) 13966-13970.

[20] N.G. Bastús, J. Comenge, V.F. Puntes, Kinetically Controlled Seeded Growth Synthesis of Citrate-Stabilized Gold Nanoparticles of up to 200 nm: Size Focusing versus Ostwald Ripening, Langmuir, 27 (2011) 11098-11105.

[21] N.G. Bastús, F. Merkoçi, J. Piella, V. Puntes, Synthesis of Highly Monodisperse Citrate-Stabilized Silver Nanoparticles of up to 200 nm: Kinetic Control and Catalytic Properties, Chem. Mater., 26 (2014) 2836-2846.

[22] S. Song, X. Wang, H. Zhang, CeO2-encapsulated noble metal nanocatalysts: enhanced activity and stability for catalytic application, Npg Asia Materials, 7 (2015) e179.

[23] L.A.J. Garvie, P.R. Buseck, Determination of Ce4+/Ce3+ in electron-beam-damaged CeO2 by electron energy-loss spectroscopy, J. Phys. Chem. Solids, 60 (1999) 1943-1947.

[24] M.C. Spadaro, P. Luches, G. Bertoni, V. Grillo, S. Turner, G. Van Tendeloo, S. Valeri, S. D'Addato, Influence of defect distribution on the reducibility of CeO2−xnanoparticles, Nanotechnology, 27 (2016) 425705.

[25] J. Piella, N.G. Bastús, V. Puntes, Size-Controlled Synthesis of Sub-10-nanometer Citrate-Stabilized Gold Nanoparticles and Related Optical Properties, Chem. Mater., 28 (2016) 1066-1075.

[26] Z.W. Seh, S. Liu, M. Low, S.-Y. Zhang, Z. Liu, A. Mlayah, M.-Y. Han, Janus Au-TiO2 Photocatalysts with Strong Localization of Plasmonic Near-Fields for Efficient Visible-Light Hydrogen Generation, Adv. Mater., 24 (2012) 2310-2314.

[27] N.G. Bastus, J. Piella, V. Puntes, Quantifying the Sensitivity of Multipolar (Dipolar, Quadrupolar, and Octapolar) Surface Plasmon Resonances in Silver Nanoparticles: The Effect of Size, Composition, and Surface Coating, Langmuir, 32 (2016) 290-300.

[28] J.L. Montaño-Priede, O. Peña-Rodríguez, U. Pal, Near-Electric-Field Tuned Plasmonic Au@SiO2 and Ag@SiO2 Nanoparticles for Efficient Utilization in Luminescence Enhancement and Surface-Enhanced Spectroscopy, J. Phys. Chem. C, 121 (2017) 23062-23071.

[29] B.K. Juluri, J. Huang, L. Jensen, Extinction, Scattering and Absorption efficiencies of single and multilayer nanoparticles, 2012.

[30] R. Jiang, B. Li, C. Fang, J. Wang, Metal/Semiconductor Hybrid Nanostructures for Plasmon-Enhanced Applications, Adv. Mater., 26 (2014) 5274-5309.

[31] S. Chervinskii, K. Koskinen, S. Scherbak, M. Kauranen, A. Lipovskii, Nonresonant Local Fields Enhance Second-Harmonic Generation from Metal Nanoislands with Dielectric Cover, Phys. Rev. Lett., 120 (2018) 113902.

[32] J. Piella, F. Merkoçi, A. Genç, J. Arbiol, N.G. Bastús, V. Puntes, Probing the surface reactivity of nanocrystals by the catalytic degradation of organic dyes: the effect of size, surface chemistry and composition, J. Mater. Chem. A, 5 (2017) 11917-11929.

[33] J. Piella, N.G. Bastús, V. Puntes, Size-controlled Synthesis of sub-10 nm Citrate-stabilized Gold Nanoparticles and Related Optical Properties, Chem. Mater., 28 (2016) 1066-1075.

[34] N.G. Bastús, J. Piella, V. Puntes, Quantifying the Sensitivity of Multipolar (Dipolar, Quadrupolar, and Octapolar) Surface Plasmon Resonances in Silver Nanoparticles: The Effect of Size, Composition, and Surface Coating, Langmuir, 32 (2016).

[35] X. Ji, X. Song, J. Li, Y. Bai, W. Yang, X. Peng, Size Control of Gold Nanocrystals in Citrate Reduction: The Third Role of Citrate, J. Am. Chem. Soc., 129 (2007) 13939-13948.

[36] F. Schulz, T. Homolka, N.G. Bastus, V. Puntes, H. Weller, T. Vossmeyer, Little adjustments significantly improve the Turkevich synthesis of gold nanoparticles, Langmuir, 30 (2014) 10779-10784.

[37] S. Kumar, K.S. Gandhi, R. Kumar, Modeling of formation of gold nanoparticles by citrate method, Industrial & Engineering Chemistry Research, 46 (2007) 3128-3136.

[38] I. Ojea-Jimenez, N.G. Bastus, V. Puntes, Influence of the Sequence of the Reagents Addition in the Citrate-Mediated Synthesis of Gold Nanoparticles, J. Phys. Chem. C, 115 (2011) 15752-15757.

[39] M.V. Kovalenko, L. Manna, A. Cabot, Z. Hens, D.V. Talapin, C.R. Kagan, V.I. Klimov, A.L. Rogach, P. Reiss, D.J. Milliron, P. Guyot-Sionnnest, G. Konstantatos, W.J. Parak, T. Hyeon, B.A. Korgel, C.B. Murray, W. Heiss, Prospects of Nanoscience with Nanocrystals, ACS Nano, 9 (2015) 1012-1057.